Research Article

Nano Research
2022, 15(6): 5410–5417

ISSN 1998-0124 CN 11-5974/O4
https://doi.org/10.1007/s12274-022-4107-y

Iodine ion modification enables Ag nanowire film with improved carrier transport properties and stability as high-performance transparent conductor

Jianfang Liu[1], Dongmei Deng[1], Yongjie Ge[2], Yaomengli Xu[1], Moxia Li[1], Bingwu Liu[1], Xidong Duan[1] (✉), Yongchun Fu[1] (✉), and Jiawen Hu[1] (✉)

[1] *Hunan Key Laboratory of Two-Dimensional Materials, Advanced Catalytic Engineering Research Center of the Ministry of Education, and College of Chemistry and Chemical Engineering, Hunan University, Changsha 410082, China*
[2] *College of Chemistry and Materials Engineering, Wenzhou University, Wenzhou 325035, China*

Received: 1 November 2021 / **Revised:** 3 December 2021 / **Accepted:** 23 December 2021

ABSTRACT

Ag nanowire (NW) film is the promising next generation transparent conductor. However, the residual long-chain polyvinylpyrrolidone (PVP, introduced during the synthesis of Ag NWs) layer greatly deteriorates the carrier transport capability of the Ag NW film and as well its long-term stability. Here, we report a one-step I^- ion modification strategy to completely replace the PVP layer with an ultrathin, dense layer of I^- ions, which not only greatly diminishes the resistance of the Ag NW film itself and that at interface of the Ag NW film and a functional layer (e.g., a current collect electrode) but also effectively isolates the approaching of corrosive species. Consequently, this strategy can simultaneously improve the carrier transport properties of the Ag NW film and its long-term stability, making it an ideal electric component in diverse devices. For example, the transparent heater and pressure sensor made from the I^--wrapped Ag NW film, relative to their counterparts made from the PVP-wrapped Ag NW film, deliver much improved heating performance and pressure sensing performance, respectively. These results suggest a facile post treatment approach for thin Ag NW film with improved carrier transport properties and long-term stability, thereby greatly facilitating its downstream applications.

KEYWORDS

Ag nanowire, transparent conductor, I^- ion modification, transparent heater, pressure sensor

1 Introduction

Transparent conductor (TC) is a key electric component in diverse photoelectric devices, such as transparent touch screen [1], organic light-emitting diode [2], and solar cell [3]. Currently, commercial TCs are usually made from indium tin oxide (ITO), which, however, faces the problems of inherent brittleness, high fabrication cost, and scarcity in indium resource [4]. To meet the increasing need of flexible photoelectric device, it is highly desirable to develop ITO-free TCs, such as thin films made from carbon nanotubes [5], reduced graphene oxide [6, 7], and metal (e.g., Ag [8] and Cu [9]) nanowires (NWs). Among these alternatives, Ag NWs appear to be the most promising alternative for ITO, because of their high flexibility, high conductivity (6.3×10^7 S/m), and excellent optical properties [10].

Currently, the well-established method of Ag NW synthesis, i.e., reduction of $AgNO_3$ with ethylene glycol, needs the introduction of long-chain polyvinylpyrrolidone (PVP) ligand to ensure anisotropic growth and effective stabilization [11, 12]. However, the introduction of PVP ligand results in an insulating PVP layer wrapping on the resultant Ag NWs, which, unfortunately, cannot be readily removed using common washing process [13]. On the one hand, the residual PVP layer greatly deteriorates the in-plane and out-of-plane carrier transport properties of the Ag NW film, i.e., the carriers transporting within and across out of the Ag NW film, respectively. This is because it greatly increases the contact resistance of the NW/NW junctions (i.e., the key limiting factor for the conductivity of the Ag NW film) and as well that at the interface of the Ag NW film and a neighboring functional layer (e.g., a current collect electrode) [14–16]. In general, the in-plane carrier transport properties of the Ag NW film can be improved upon solid bonding of the NW/NW junctions using various welding strategies, such as thermal [17] and light welding [18], capillary-force welding [19], and electrochemical method [20]. However, these welding strategies are unable to remove the residual PVP ligands from the sites other than the NW/NW junctions, thereby furnishing no positive impact on the out-of-plane carrier transport properties of the Ag NW film. Prompted by this understanding, we have developed a series of post treatment strategies, including $NaBH_4$ treatment [14], electrochemical cleaning [15], and plasma cleaning [16], to completely remove the residual PVP ligands. Although greatly favoring the carrier transport properties of the Ag NW film, the removal of PVP ligand fully exposes the bare surfaces of the Ag NWs, therefore increasing their corrosion risk in ambient air [14]. On the other hand, the residual PVP layer itself, contrary to expectations, also deteriorates the long-term stability of the Ag

Address correspondence to Xidong Duan, xidongduan@hnu.edu.cn; Yongchun Fu, ycfu@hnu.edu.cn; Jiawen Hu, jwhu@hnu.edu.cn

NW film because of its uncompacted surface configuration [21] and great affinity to water [14]. To address this issue, a series of protective coatings have been exploited, including coatings of carbonaceous shell [21], graphene [22], graphene oxide [23], metal (e.g., Au [24] and Ni [25]) and metal oxide (e.g., SnO_2 [26], TiO_2 [27], and Hf:ZnO [28]), organic sulfhydryl compound (e.g., 11-mercaptoundecanoic acid [29], dodecanethiol (DT) [14], and 2-mercaptobenzimidazole [30]), and C_xF_y polymer [31]. However, a thick insulating coating may deteriorate not only the out-of-plane carrier transport properties of the Ag NW film but also its transmittance because of the film's enhanced light scattering.

Clearly, an efficient coating needs to compromise the long-term stability of the Ag NW film and its (especially, the out-of-plane) carrier transport properties and transparency. Previously, Ning et al. and Chu et al. have found that surface modification with halide ligands can greatly improve the air stability of semiconductor dots [32] and Ag NWs [33], respectively. Inspired by these progresses, herein, we develop a I^- ion modification strategy to completely replace the residual PVP layer with an ultrathin, dense layer of I^- ions, with the following expectations. The replacement of a thick PVP layer with an ultrathin (at sub-nanometer scale) ion layer would greatly improve the carrier transport properties of the Ag NW film because it greatly diminishes the contact resistance at the NW/NW junctions and that at the interface between an Ag NW film and its neighboring functional layer. Owing to its great affinity to metal and single atomic size, the I^- ion ligand would readily form a dense and ultrathin protective coating effectively against the approaching of external corrosive species, thereby improving the long-term stability of the Ag NW film while not deteriorating its transparency. Therefore, this simple post treatment shows great practical potential in a continuous fabrication line for high-performance Ag NW film and the downstream devices made from it.

2 Experimental section

2.1 Materials

$AgNO_3$ (AR), PVP (K-30), $CuCl_2$ (AR), ethylene glycol (AR), KI (AR), DT (98%), $PbNO_3$ (AR), and $NaBH_4$ (98%) were purchased from Sinopharm Chemical Reagent Co., Ltd. (Shanghai, China). Benzothiazole (BT) (≥ 96.0%) and CH_3CSNH_2 were purchased from Shanghai Macklin Biochemical Co., Ltd. (China). Tetramethylammonium hydroxide (TMAH) was purchased from Changchun Yinghua Co., Ltd. (China). All other chemicals were obtained from native suppliers. Photoresist (SPR220-7.0), polydimethylsiloxane (PDMS), polyethylene terephthalate (PET) film (thickness, 0.125 mm), cotton fabric, commercial interdigitated electrodes (IDEs) with 20 pairs of microelectrode fingers (width, spacing, and length: 90 μm, 110 μm, and 6 mm) on PET substrate, and Si/SiO_2 slide were purchased from Suzhou Ruicai Semiconductor Co., Ltd. (China), Dow Corning Corp. (USA), Shanghai Feixia Rubber and Hardware Co., Ltd. (China), Shenzhen Balingzan Electronic Business Co., Ltd. (China), Huizhou Xinwenxiong Trading Co., Ltd. (China), and Suzhou Jingxi Electronic Co., Ltd. (China), respectively. Ultrapure water (≥ 18.2 MΩ·cm) was purified from a RS2200QUV-PURIST system (Shanghai Rephile Bioscience Co., Ltd., China) and used for all experiments.

2.2 Synthesis of Ag NWs, fabrication of Ag NW film, its surface modification with I^- ions, and stability tests

Polyol reduction method [11] was used to synthesize the Ag NWs. The resultant PVP-wrapped Ag NWs were separated from the reaction mixture by adding acetone, further cleaned upon 3 cycles of centrifugation and redispersion in ethanol, and finally stored in ethanol to form a stock dispersion (0.73 mg/mL). They have an average length and diameter of 36.15 ± 0.98 μm and 97.10 ± 2.27 nm (Fig. S1 in the Electronic Supplementary Material (ESM)), respectively.

To fabricate PVP-wrapped Ag NW film, diluted Ag NW dispersion (500 μL, 0.24 mg/mL) was spin coated on a PET substrate (3 cm × 3 cm), followed by natural drying in air. Surface modification of the PVP-wrapped Ag NW film with a I^- ion layer was readily accomplished by immersing in a KI solution (10 mL, 0.048 mmol/L) for 5 min, followed by sequentially washing with water and ethanol and finally drying in a N_2 flow. To ensure a dense I^- ion layer, the amount of the I^- ions is sufficient for a saturated monolayer adsorption, whose calculation is detailed in the ESM. For comparison, the PVP-wrapped Ag NW film was also modified with a DT (or BT) layer, accomplished by immersing the surface-cleaned Ag NW film (achieved upon treatment of the pristine film in a 0.1 M $NaBH_4$ solution for 2 min [14]) in a 0.5 M DT (or 0.17 M BT [34]) solution in ethanol for 5 min, followed by washing and drying as the procedures described above. For reliable comparison, the areal density of Ag NWs in these compared Ag NW films was adjusted to be nearly identical. That can be readily achieved by preparing them from the almost equally transparent (T = 89% ± 1% @ 550 nm) PVP-wrapped Ag NW films (prepared under identical spin coating conditions using the same batch of dispersion of PVP-wrapped Ag NWs as ink).

The long-term stability test of the PVP-, I^--, DT-, and BT-wrapped Ag NW films was performed by exposing in spring air (room temperature, ~ 25 °C; humidity, ~ 30%) and in an H_2S atmosphere (created by containing 0.01 M CH_3CSNH_2 + 0.01 M H_2SO_4 in a sealed desiccator) for different durations. During exposing, the conductivity of each film was intermittently monitored, from which the degradation extent of the Ag NW film can be judged.

2.3 Fabrication of single Ag NW device with a NW/NW junction

The contact resistance of a NW/NW junction was measured from a single Ag NW device with a NW/NW junction. To construct the single Ag NW device, Ag NW dispersion (100 μL, 0.15 mg/mL) was spin coated onto a Si/SiO_2 substrate (1 cm × 1 cm) at 1,200 rpm for 20 s, followed by drying and spin coating a positive photoresist (SPR220-7.0, 500 μL) at 7,000 rpm for 40 s. Upon heating in air on a hotplate at 115 °C for 300 s, single crossed Ag NWs with a NW/NW junction were positioned and patterned at their terminals using the standard lithography process on a lithography machine (UTA-IA-SET, Arms system, Japan), followed by development in a TMAH solution for 40 s to expose the patterned areas. Upon rinsing with pure water and drying in a N_2 blow, Ag pads (thickness, 60 nm) were deposited onto the patterned areas as electrodes in a JSD 300 vacuum evaporator (Anhui Jiashuo Vacuum Science and Technology Co., Ltd., China). Finally, single Ag NW device defined with Ag electrodes was obtained when the photoresist where the area is not patterned was dissolved away in acetone.

2.4 Fabrication of transparent heater and pressure sensor

Transparent heater was fabricated using PVP- and I^--wrapped Ag NWs films as the heating component. To this end, the two ends of the Ag NW film (3 cm × 3 cm) were cast with silver paste, followed by adhering copper tape as electric connector. To ensure reliable comparison, the two Ag NW films have nearly identical

transparency (~ 86.51 *T*% at 550 nm).

Pressure sensor was fabricated using Ag NW film embedded in a cotton fabric (10 mm × 20 mm) as the sensing component. To this end, the sensing component was sandwiched between a protective PDMS film (~ 500 μm thickness) and a commercial IDE (as current collector). The sensing component was prepared by sufficiently cleaning the cotton fabric, treating it to hydrophilicity in a O_2 plasma (SmartPlasma system, Plasma Technology GmbH, Germany), immersing in an Ag NW dispersion (5 mL, 0.3 mg/mL) for 30 min, and finally drying at 80 °C. During pressure sensing, different weights were gently placed on the sensor with a defined dimension, from which the pressure loading can be readily calculated.

2.5 Characterization

Scanning electron microscopy (SEM) images and transmission electron microscopy (TEM) images were obtained on a TESCAN MIRA3 LMH microscope equipped with an energy-dispersive X-ray spectrometer (EDS) (TESCAN Co., Ltd., Czech Republic) and a Titan G260-300 microscope (FEI, America), respectively. To increase the electron density in the PVP layer and thereby improve its contrast in the SEM images, the PVP-wrapped Ag NWs were negatively stained in a 1 wt.% $Na_3O_4PW_{12}$ solution for 5 min. Raman spectra were measured on an inVia Reflexer spectrometer (Renishaw, UK) using a 532 nm laser as the excitation source. X-ray photoelectron spectroscopy (XPS) spectra were recorded on an Axis Supra system with an Al K*α* source (1,486.69 eV) (Shimadzu-Kratos, UK). X-ray diffraction (XRD) patterns were obtained on an XRD-6100 diffractometer with a Cu-K*α* radiation (Shimadzu, Japan). The transmittance and sheet resistance of the Ag NW film were measured on a UV-1800 ultraviolet–visible (UV–vis) spectrometer (Shimadzu, Japan) and on an RTS-9 four-point probe instrument (Guangzhou Four-probe Scientific Co., Ltd., China), respectively. Current–voltage (*I*–*V*) response of the single Ag NW device was monitored using an Agilent B1500A semiconductor parameter analyzer. The temperature and thermal images of the transparent heater were obtained using an infrared thermal camera (Fotric 322Pro, Fotric, America). The *I*–*V* curves of the pressure sensor under different pressure loads were recorded using a B2912A precision source/measure unit (Keysight, America). Cyclic voltammetry (CV) and electrochemical impedance spectroscopy (EIS) measurements were conducted in a three-electrode electrochemical cell using an Autolab PGSTAT-302 electrochemical workstation (Metrohm, Switzerland). The EIS spectra were measured at open circuit potential by superimposing a sinusoidal signal with 10 mV amplitude over a frequency range of 100 kHz–0.01 Hz. For these electrochemical measurements, the working electrode was prepared by dropping the Ag NW dispersion (5 μL, ~ 0.73 mg/mL) on a glassy carbon (GC) electrode (3 mm, in diameter), followed by drying in air. A Pt wire and a Hg/Hg_2SO_4 electrode were used as the counter electrode and the reference electrode, respectively.

3 Results and discussion

3.1 Surface modification of the Ag NWs with I^- ions and their characterization

During the synthesis of Ag NWs, the introduction of PVP ligand unavoidably results in an insulating PVP layer wrapping on the Ag NWs. The residual PVP layer, on the one hand, creates high contact resistance at the NW/NW junctions and also high contact resistance at the interface between the Ag NW film and its neighboring functional layer (e.g., a current collect electrode), thereby greatly deteriorating the in-plane and out-of-plane carrier transport properties of the Ag NW film, respectively [14–16]. On the other hand, the residual PVP layer also deteriorates the long-term stability of the Ag NW film because of its uncompacted surface configuration [21] and great affinity to water [14]. To overcome these problems, we hereby exploit the ultra-small I^- ions to completely replace the long-chain PVP layer to produce an ultrathin, dense layer of I^- ions, expecting to simultaneously improve the carrier transport properties of the Ag NW film and its long-term stability, while not affecting its transparency. Figure 1 illustrates the surface modification process and its impact on the carrier transport properties of the Ag NW film and its long-term stability. The PVP ligands weakly bind to the metal surface via their carbonyl groups [35]. Therefore, they are possible to be replaced by other ligands which show a stronger affinity to the Ag NWs, e.g., I^- ions, as a result of the formation of the strong Ag–I bond.

The successful replacing of the PVP layer by a I^- ion layer was confirmed using SEM and TEM studies. Figure 2 shows the SEM and TEM images for the pristine PVP-wrapped Ag NWs and that upon a I^- ion modification process. The PVP-wrapped Ag NWs feature a light layer around their surfaces (Fig. 2(a)). As more clearly revealed by the TEM image, the light layer is a ~ 2.3 nm amorphous layer neighboring the crystalline area of the Ag NWs (Fig. 2(b)). Upon a I^- ion modification process, the light amorphous layer was completely removed, exposing the clear

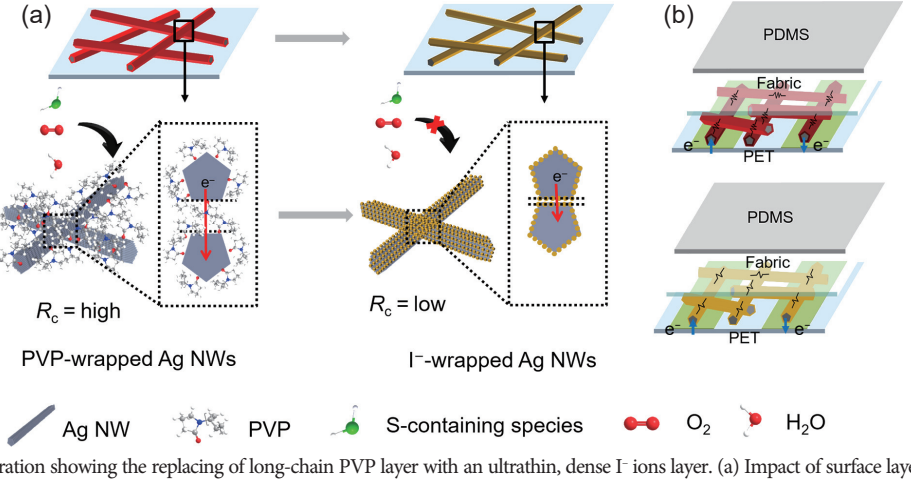

Figure 1 Schematic illustration showing the replacing of long-chain PVP layer with an ultrathin, dense I^- ions layer. (a) Impact of surface layer on the in-plane carrier transport of the Ag NW film and its long-term stability. (b) Impact of the surface layer on the in-plane and out-of-plane carrier transport of the Ag NW film in a pressure sensor.

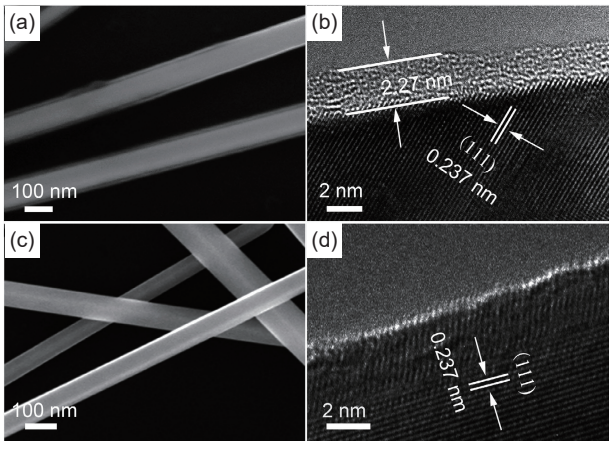

Figure 2 Morphology characterization of the Ag NWs. (a) SEM and (b) TEM images of the PVP-wrapped Ag NWs. (c) SEM and (d) TEM images of the I^--wrapped Ag NWs.

crystalline area of the Ag NWs (Figs. 2(c) and 2(d)). Cleary, the PVP layer can be completely replaced upon a simple KI solution treatment process, as can be further confirmed using Raman, XPS, and XRD studies. Figure 3(a) shows the Raman spectra for the PVP- and I^--wrapped Ag NWs. The Raman spectrum for the PVP-wrapped Ag NWs shows two distinct peaks at 233 and 1,658 cm^{-1}, which are assigned to the Ag–O stretching (ν_{Ag-O}) mode [36] and the C=O stretching ($\nu_{C=O}$) mode of the PVP ligand, respectively. In contrast, they are absent in the Raman spectrum for the I^--wrapped Ag NWs, on which an additional intense ν_{Ag-I} peak appears at 108 cm^{-1}. Additionally, the XPS spectrum for the I^--wrapped Ag NWs also shows two additional distinct binding peaks at 618.1 (I $3d_{5/2}$) and 629.5 eV (I $3d_{3/2}$) (Fig. 3(b)) [37]. Moreover, high-resolution XPS spectra show that upon a I^- ion modification process, the binding energy for the Ag $3d_{5/2}$ peak (367.4 eV) and the Ag $3d_{3/2}$ peak (373.4 eV) shifts to a relatively higher value (Fig. 3(c)), because of the weaker electron-donating effect from the adsorbed I^- ions [38]. These Raman and XPS studies, from a molecule level, further confirm the removal of the PVP layer and the successful formation of a I^- ion layer on the Ag NWs. To reveal whether the surface modification impacts the crystal structure of the Ag NWs or not, Fig. 3(d) compares the XRD patterns of the PVP- and I^--wrapped Ag NWs. The two XRD patterns both show four distinct diffraction peaks at 38.1°, 44.2°, 64.4°, and 77.42°, corresponding to the (111), (200), (220), and (311) planes of the face-centered cubic (fcc) silver crystal (PDF No. 04-0783), respectively [39]. The two types of Ag NWs

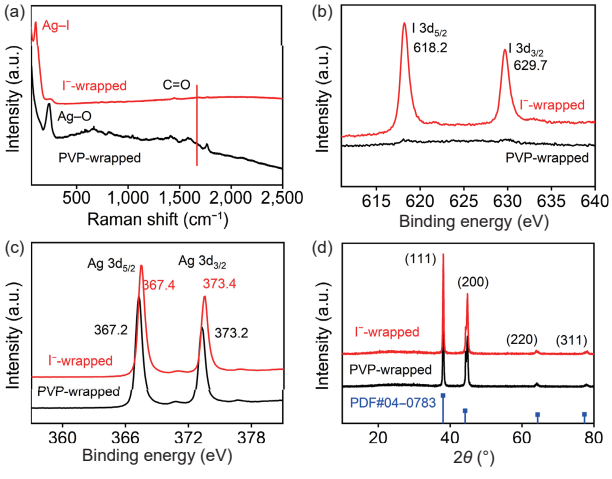

Figure 3 Spectral characterization of the PVP- and I^--wrapped Ag NWs. (a) Raman spectra, (b) XPS spectra of I 3d, (c) XPS spectra of Ag 3d, and (d) XRD patterns.

essentially have identical XRD features, suggesting that the surface modification process only involves the outmost surface atoms on the Ag NWs, not influencing their bulk crystalline structure and thereby their inherent conductivity.

The coating quality of the I^- ion layer was examined using CV and underpotential deposition (UPD) studies because they both are surface-sensitive techniques, reflecting more electrochemical properties of the surface than that of the bulk electrode. Figure S2(a) in the ESM shows the CV curves of the PVP- and I^--wrapped Ag NWs in 0.5 M $NaClO_4$ solution. The CV curve for the PVP-wrapped Ag NWs shows a distinct oxidation peak at 0.10 V and a reduction peak at −0.14 V, signaling the formation of a Ag_2O layer and its subsequent reduction back to the metal state of Ag, respectively. These CV behaviors qualitatively agree with the typical electrochemical behaviors of a polycrystalline Ag electrode (Fig. S2(b) in the ESM) [40]. In contrast, the CV curve for the I^--wrapped Ag NWs shows a much-depressed oxidation peak at −0.10 V and a similarly depressed reduction peak at −0.23 V. Clearly, although with a thicker thickness and because of its uncompacted surface configuration [21], the residual PVP layer itself unlikely effectively limits the adsorption of H_2O to the bare Ag surface sites, which is typically identified as the first step for the surface oxidation of Ag metal in a neutral electrolyte. Upon the replacing, the resultant I^- ion layer clearly forms a dense (although not pinhole-free), protective coating so that it can effectively limit the approaching of the relatively large oxygen-containing H_2O species. The same is true even for smaller single atomic ions, as can be confirmed using UPD studies. Figure S2(c) in the ESM displays the CV behaviors of electrodeposition of Pb^{2+} ions on the PVP- and I^--wrapped Ag NWs. Referring to the typical UPD behaviors of Pb^{2+} ions on polycrystalline Ag electrode (Fig. S2(d) in the ESM), the first couple peaks at −0.77 and −0.66 V are assigned to the UPD of Pb^{2+} ions on the surface of Ag NWs and the stripping of the UPD monolayer of Pb, respectively. The second couple peaks at −0.93 and −0.82 V are assigned to the bulk deposition of Pb^{2+} ions and the stripping of the bulk Pb, respectively [41]. Compared with the PVP-wrapped Ag NWs, the I^--wrapped Ag NWs as well deliver much weaker current densities for the two couples of deposition/stripping peaks, thereby further confirming the dense nature of the I^- ion layer against the approaching of external species. Not only that, this I^- ion layer has been extensively used as the insulating layer for limiting the charge transfer between π-conjugated organic molecules and a metal substrate and thereby decoupling their electronic interaction [42].

3.2 Impact of I^- ion modification on the carrier transport properties of the Ag NW film

Because of its single atomic thickness, the ultrathin I^- ion layer, upon replacing of the thick PVP layer, can greatly improve the carrier transport properties of the Ag NW film. The improved in-plane carrier transport properties of the I^--wrapped Ag NW film can be readily revealed by measuring the film's sheet resistance and the contact resistance of a single NW/NW junction. Figure 4(a) shows the sheet resistance and transmittances for three PVP-wrapped Ag NW films before and after I^- ion modification. For the three PVP-wrapped Ag NW films with different initial transmittances, the formation of a I^- ion layer diminished their initial sheet resistance from 164, 115, and 78 to 60, 43, and 32 Ω/sq, respectively, while not influencing their transmittance. This improved conductivity (and in turn improved in-plane carrier transport properties) is attributed to the diminished contact resistance at the NW/NW junctions, which can be measured from a single Ag NW device with a NW/NW junction (Fig. 4(b)). Figure 4(c) shows the typical *I*–*V* curves measured from single PVP- and I^--wrapped Ag NW devices, from which the contact resistance at the NW/NW junction can be readily extracted using the Ohm's law. Replacing the PVP layer with a I^- ion layer

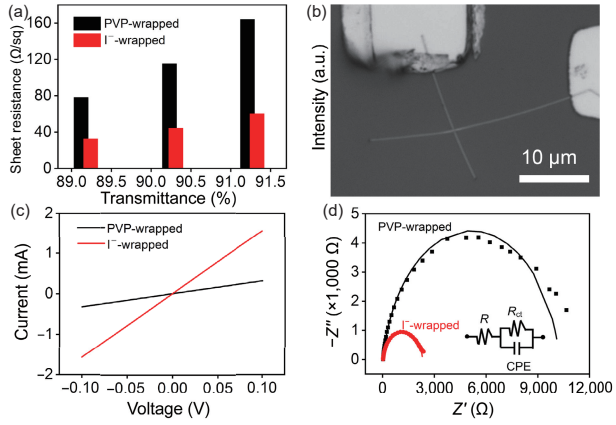

Figure 4 Impact of the replacing of PVP layer with a dense, ultrathin I^- ion layer on the carrier transport properties of the Ag NW film and its transparency. (a) Sheet resistance and transmittance of the PVP- and I^--wrapped Ag NW films. (b) Typical optical image of a single Ag NW device with a NW/NW junction. (c) *I*–*V* curves measured from the single Ag NW device. (d) Nyquist plots and corresponding equivalent circuit (inset) of the PVP- and I^--wrapped Ag NWs (supported on a glass carbon electrode) in 2 mM $K_3Fe(CN)_6/K_4Fe(CN)_6$ + 0.5 M $NaClO_4$ solution.

typically diminished the contact resistance at the NW/NW junction from 312.5 to 64.1 Ω, thereby accordingly increasing the in-plane current by 4.88 times (Fig. 4(c)). The improved out-of-plane carrier transport properties of the I^--wrapped Ag NW film can be vividly revealed by monitoring its EIS behaviors in a solution. Figure 4(d) shows the Nyquist plots and the corresponding equivalent circuit (inset) for the PVP- and I^--wrapped Ag NWs in 2 mM $K_3Fe(CN)_6/K_4Fe(CN)_6$ + 0.5 M $NaClO_4$ solution. For both types of Ag NWs, only a semicircle appears in the high frequency region, lacking the typical Warburg impedance in middle frequency region and the capacitive line in the lower frequency region [15]. These observations suggest that a large charge transfer resistance (Table S1 in the ESM) dictates the reaction kinetics for the $Fe(CN)_6^{3-/4-}$ couple, which can be reasonably understood because during reaction the redox couples need transport across the coating layer on the Ag NW film. From the intercept of the *Z*' axis, the heterogeneous electron transfer resistance (R_{ct}) extracted is 10.22 and 2.295 KΩ for the PVP- and I^--wrapped Ag NWs, respectively. Also clearly, the I^- ion layer as well can substantially reduce the resistance at the Ag NW film/solution interface, resulting in improved out-of-plane carrier transport properties, which would greatly facilitate the applications of the Ag NW film, especially, in stacked device constructed from it.

3.3 Impact of I^- ion modification on the stability of the Ag NW films

The dense nature of the I^- ion layer suggests that the I^- ion can serve as efficient corrosion inhibitor to largely improve the long-term stability of the Ag NW film. To this end, we have first compared the impact of PVP ligand, I^- ion, BT [34], and DT [14] (two typical organic corrosion inhibitors, which can form a dense self-assembled monolayer on metal surface) on the stability of the Ag NW film in spring air. Upon exposure for 40 days, the sheet resistance of the PVP-, BT-, DT-, and I^--wrapped Ag NW films with a nearly identical transparence (T = 89% ± 1% @ 550 nm) gradually increases from 103, 62, 49, and 43 to 201, 69, 63, and 57 Ω/sq (Fig. 5(a)). Although the four Ag NW films all gradually corroded, the corrosion extent is apparently comparable for the latter three Ag NW films. Their final SEM images show that long-term exposure gradually roughens the surface of the Ag NWs (Figs. 5(b)–5(e)), especially for the Ag NWs wrapped with a PVP layer because of its inferior protective effect (Figs. S2(a) and S2(c) in the ESM). EDS analysis reveals that the resultant four Ag NW films all contain S element (Fig. 5(f)), whose content is 8.94%, 0.41%, 0.83%, and 1.95% for the PVP-, BT-, DT-, and I^--wrapped Ag NW films, respectively. The S contents in these corroded Ag NW films are apparently along with their degradation trend, implying that the S-containing species plays a key role for their corrosion [43]. These results reveal that although I^- ion layer is the thinnest coating among the four coatings examined, it unexpectedly exhibits comparable corrosion-resistant capability to that from the relatively thick BT and DT layer. To accelerate the corrosion rate, we have further compared the impact of the PVP ligand, I^- ion, BT, and DT on the stability of the Ag NWs exposed in a H_2S atmosphere. Under these severely corrosive conditions, the I^- ion layer still exhibited largely improved corrosion-resistant capability, only slightly less inferior to that from the BT and DT layer but far outperforming that from PVP layer, as can be confirmed by examining the conductivity, surface morphology, and S content for the PVP-, BT-, DT-, and I^--wrapped Ag NW films upon exposure in H_2S for 24 h (Fig. S3 in the ESM). In Table S2 in the ESM, we have further compared the conductivity and stability of the Ag NW films treated using different methods. This more extensive comparison still confirms the advantage of the I^- ion layer as an efficient corrosion inhibitor in terms of the stability and conductivity of the Ag NW film.

3.4 Applications of the I^--wrapped Ag NW films in transparent heater and pressure sensor

With largely improved carrier transport properties and stability,

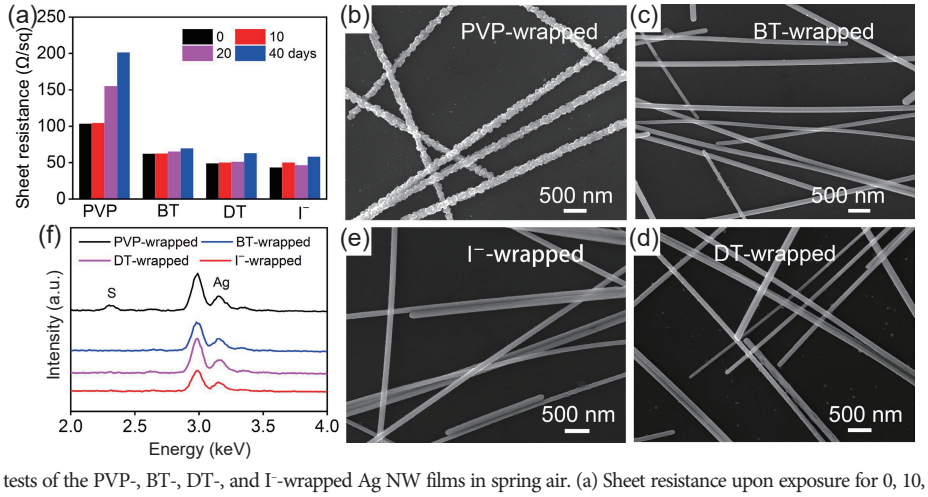

Figure 5 Anticorrosion tests of the PVP-, BT-, DT-, and I^--wrapped Ag NW films in spring air. (a) Sheet resistance upon exposure for 0, 10, 20, and 40 days. (b)–(e) SEM images upon exposure for 40 days. (f) EDS spectra upon exposure for 40 days.

the I^--wrapped Ag NW film may serve as an ideal electric component for diverse devices. To demonstrate its practical potential, we have first constructed a transparent heater (dimensions, 3 cm × 3 cm) from the I^--wrapped Ag NW film. Compared with its control counterpart made from the PVP-wrapped Ag NW film, the transparent heater made from the I^--wrapped Ag NW film can increase to a higher temperature at each increasing/decreasing voltage step and also delivers a wider working temperature range (29.1–71.4 vs. 27.9–56.2 °C for its control counterpart) at the same voltage range of 1–5 V (Fig. 6(a)). Furthermore, although the two heaters both can increase to a steady temperature within 25 s, the transparent heater made from the I^--wrapped delivers not only a faster heating rate (0.28, 0.74, 1.32, and 1.95 vs. 0.12, 0.38, 0.73, and 1.16 °C/s for its control counterpart at an applied voltage of 2, 3, 4 and 5 V, respectively) but also a higher steady temperature at different applied voltages (Figs. 6(b)–6(d)). This improved performance can be reasonably attributed to the higher conductivity of I^--wrapped Ag NW film, which enables efficient current-to-heat conversion, far outperforming that from the PVP-wrapped Ag NW film. Also clearly, the two transparent heaters both can steadily operate for a long duration of 1,800 s and repeatedly operate for at least 10 cycles, demonstrating high long-term operation stability and recycling stability (Figs. 6(e) and 6(f)). This is because the nanostructure of the flexible Ag NW film is robust enough to withstand the applied voltage when it is within the safe working range. We have then constructed a pressure sensor with a sandwiched PDMS/Ag NW film/IDE configuration (Fig. 7(a)), in which Ag NWs were embedded in a supporting cotton fabric, forming an Ag NW film with randomly separated Ag NWs. When applied with increasing pressure loading, more and more Ag NWs contact with each other, and so do they and the current collector (i.e., the IDEs). This in turn generates increasing electron transport pathways for the current to signal the pressure loading [44, 45]. For the two pressure sensors made from PVP- (sensor 1) and I^--wrapped Ag NW film (sensor 2), their current collected linearly increases with the applied voltage at different pressure loadings, suggesting only Ohm resistance in the sensor (Fig. 7(b)). Under the same pressure loading, e.g., 24.5 kPa, the current collected from sensor 2 (Fig. 7(c)) is 1.27 times higher than that collected from sensor 1 (Fig. 7(b)). This improved current collect efficiency can be reasonably understood from the structure configuration of the pressure sensor (Fig. 7(a)), whose overall resistance R_{total} can be expressed as $R_{total} = R_{Ag\ NW\ film} + R_{Ag\ NW\ film/IDE}$. Here, $R_{Ag\ NW\ film}$ is the resistance of the Ag NW film embedded in the fabric and $R_{Ag\ NW\ film/IDE}$ is the contact resistance at the Ag NW film/IDE interface. They, as revealed previously (Fig. (4)), both can be largely decreased upon replacing of a thick PVP layer with an ultrathin I^- ion layer, thereby synergistically decreasing the R_{total} of the pressure sensor 2. As a result, the

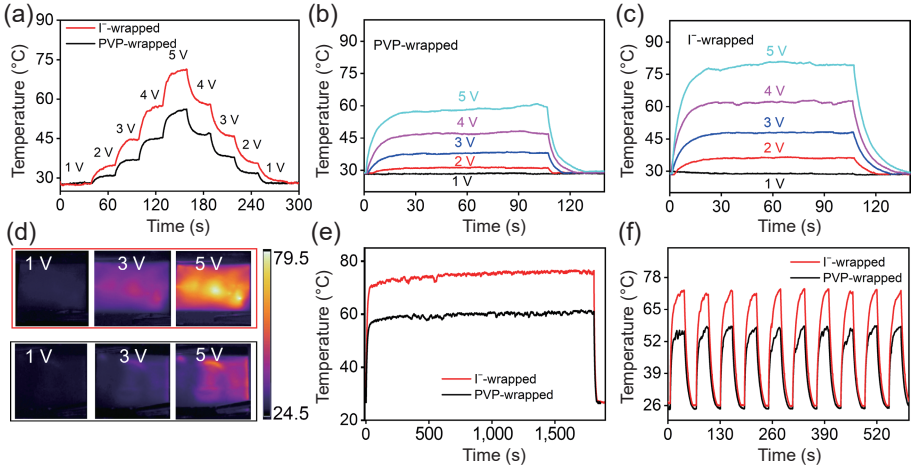

Figure 6 Heating performance of the transparent heater made from PVP- and I^--wrapped Ag NW films. (a) Temperature evolution of the transparent heater at stepwise increasing/decreasing applied voltages. (b) and (c) *T*–*V* curves of the transparent heaters made from (b) PVP- and (c) I^--wrapped Ag NW films at different applied voltages. (d) Infrared thermal images of transparent heater made from (top panels) I^-- and (bottom panels) PVP-wrapped Ag NW film at different applied voltages. (e) Long-term stability tests at an applied voltage of 5 V. (f) Cycling stability tests at an applied voltage of 5 V for 10 cycles of heating/cooling (duration, 30 s/30 s).

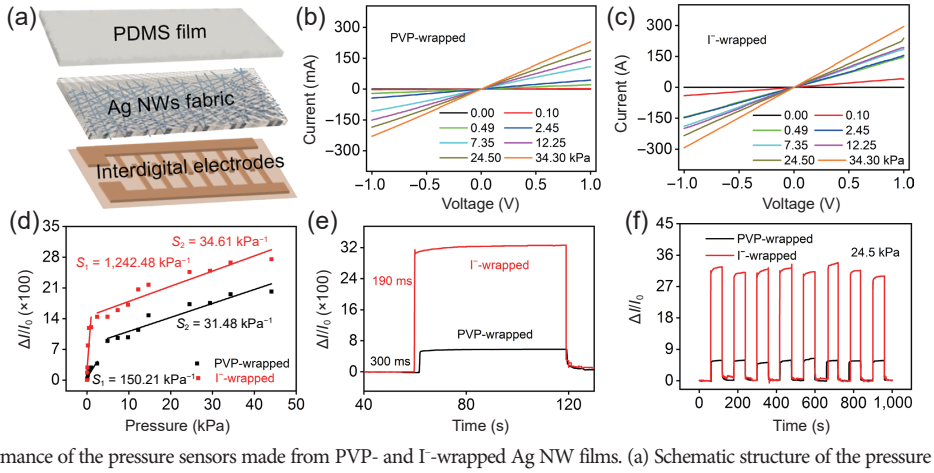

Figure 7 Sensing performance of the pressure sensors made from PVP- and I^--wrapped Ag NW films. (a) Schematic structure of the pressure sensor. (b) and (c) *I*–*V* curves of the pressure sensors made from (b) PVP- and (c) I^--wrapped Ag NW films under various applied pressures. (d) Relative current response to external pressure. (e) Response time under a pressure of 24.5 kPa. (f) Stability tests under an intermittently applied pressure of 24.5 kPa.

current collected on sensor 2 is more sensitive to external pressure loading, as can be revealed by the term of sensitivity (S). Here, S is defined as $S = \Delta I/I_0/p$, where $\Delta I = I - I_0$ is current variation and I and I_0 are the current collected with and without the pressure loading of p, respectively. Notably, pressure sensor 2 shows a sensitivity of 1,242.48 and 34.61 kPa^{-1} in the loading range of 0.00–0.98 and 2.45–44.10 kPa, respectively, both of which outperform that (150.21 and 31.78 kPa^{-1}, respectively) of pressure sensor 1 (Fig. 7(d)). Furthermore, pressure sensor 2 also shows a faster response time of 190 ms at a representative pressure loading of 24.50 kPa (vs. 300 ms for pressure sensor 1), thereby ensuring flexible sensing in a timely manner (Fig. 7(e)). For the two pressure sensors, they both show high stability, as revealed by observing their current intensity and its recovery upon loading and unloading of the pressure (24.50 kPa) for 8 cycles. Table S3 in the ESM compares the performance of the pressure sensors made from different materials, in which the pressure sensor made from I^--wrapped Ag NW film is still among the best value. These results show the great practical potential of I^--wrapped Ag NW film as key electric component in transparent heater, pressure sensor, and beyond.

4 Conclusions

In summary, we report a feasible and low-cost post treatment approach to completely replace the long-chain PVP layer wrapping on the Ag NW film with an ultrathin and dense I^- ion layer. As a result, the I^- ion layer largely diminishes the contact resistance at the NW/NW junctions and as well that at the interface between the Ag NW film and its neighboring functional layer, thereby largely improving the carrier transport properties of the Ag NW film, while not influencing its transmittance. Furthermore, unlike the PVP layer which has an uncompacted surface configuration, the I^- ion layer is ultrathin and dense so that it can effectively limit the approaching of external corrosive species to ensure largely improved long-term stability to the Ag NWs. With these merits, the I^--wrapped Ag NW film can serve as ideal electric component in diverse devices, resulting in greatly improved performance, as confirmed by comparing the performance of the transparent heater and pressure sensor made from the PVP- and I^--wrapped Ag NW film. These results demonstrate a rapid (within a few minutes), low-cost post treatment approach, which can simultaneously improve the carrier transport properties and long-term stability of the Ag NW film, thereby greatly facilitating its downstream applications.

Acknowledgements

The authors greatly thank the financial support from the National Natural Science Foundation of China (Nos. 21872047, 21673070, and 22072039) and Hunan Key Laboratory of Two-Dimensional Materials (No. 2018TP1010).

Electronic Supplementary Material: Supplementary material (SEM images of PVP-wrapped Ag NWs and their length and diameter distribution, electrochemical characterization of PVP- and I^--wrapped Ag NWs, accelerated sulfurization tests in a H_2S atmosphere, electrochemical parameters extracted from the EIS data for the PVP- and I^--wrapped Ag NWs films, comparison of the stability of the Ag NW film upon different post treatments, comparison of the performance of flexible pressure sensors, and calculation of the amount of I^- ions required for a saturated monolayer coverage on the surfaces of Ag NWs) is available in the online version of this article at https://doi.org/10.1007/s12274-022-4107-y.

References

[1] Kim, S. J.; Phung, T. H.; Kim, S.; Rahman, M. K.; Kwon, K. S. Low-cost fabrication method for thin, flexible, and transparent touch screen sensors. *Adv. Mater. Technol.* **2020**, *5*, 2000441.

[2] Lee, S.; Bae, H. W.; Lampande, R.; Yang, H. I.; Oh, J. S.; Kwon, J. H. Ultrathin Ag transparent conducting electrode structure for next-generation optoelectronic applications. *ACS Appl. Electron. Mater.* **2020**, *2*, 1538–1544.

[3] Zhang, Y. K.; Ng, S. W.; Lu, X.; Zheng, Z. J. Solution-processed transparent electrodes for emerging thin-film solar cells. *Chem. Rev.* **2020**, *120*, 2049–2122.

[4] Angmo, D.; Krebs, F. C. Flexible ITO-free polymer solar cells. *J. Appl. Polym. Sci.* **2013**, *129*, 1–14.

[5] Wu, Z. C.; Chen, Z. H.; Du, X.; Logan, J. M.; Sippel, J.; Nikolou, M.; Kamaras, K.; Reynolds, J. R.; Tanner, D. B.; Hebard, A. F. et al. Transparent, conductive carbon nanotube films. *Science* **2004**, *305*, 1273–1276.

[6] Lee, D. W.; Hong, T. K.; Kang, D. W. O.; Lee, J.; Heo, M.; Kim, J. Y.; Kim, B. S.; Shin, H. S. Highly controllable transparent and conducting thin films using layer-by-layer assembly of oppositely charged reduced graphene oxides. *J. Mater. Chem.* **2011**, *21*, 3438–3442.

[7] Moon, I. K.; Lee, J.; Ruoff, R. S.; Lee, H. Reduced graphene oxide by chemical graphitization. *Nat. Commun.* **2010**, *1*, 73.

[8] Hu, L. B.; Kim, H. S.; Lee, J. Y.; Peumans, P.; Cui, Y. Scalable coating and properties of transparent, flexible, silver nanowire electrodes. *ACS Nano* **2010**, *4*, 2955–2963.

[9] Liu, G. Z.; Wang, J.; Ge, Y. H.; Wang, Y. J.; Lu, S. Q.; Zhao, Y.; Tang, Y.; Soomro, A. M.; Hong, Q. M.; Yang, X. D. et al. Cu nanowires passivated with hexagonal boron nitride: An ultrastable, selectively transparent conductor. *ACS Nano* **2020**, *14*, 6761–6773.

[10] Liu, C. H.; Yu, X. Silver nanowire-based transparent, flexible, and conductive thin film. *Nanoscale Res. Lett.* **2011**, *6*, 75.

[11] Sun, Y. G.; Mayers, B.; Herricks, T.; Xia, Y. N. Polyol synthesis of uniform silver nanowires: A plausible growth mechanism and the supporting evidence. *Nano Lett.* **2003**, *3*, 955–960.

[12] Jharimune, S.; Pfukwa, R.; Chen, Z. F.; Anderson, J.; Klumperman, B.; Rioux, R. M. Chemical identity of poly (N-vinylpyrrolidone) end groups impact shape evolution during the synthesis of Ag nanostructures. *J. Am. Chem. Soc.* **2021**, *143*, 184–195.

[13] Hwang, J.; Shim, Y.; Yoon, S. M.; Lee, S. H.; Park, S. H. Influence of polyvinylpyrrolidone (PVP) capping layer on silver nanowire networks: Theoretical and experimental studies. *RSC Adv.* **2016**, *6*, 30972–30977.

[14] Ge, Y. J.; Duan, X. D.; Zhang, M.; Mei, L.; Hu, J. W.; Hu, W.; Duan, X. F. Direct room temperature welding and chemical protection of silver nanowire thin films for high performance transparent conductors. *J. Am. Chem. Soc.* **2018**, *140*, 193–199.

[15] Ge, Y. J.; Liu, J. F.; Liu, X. J.; Hu, J. W.; Duan, X. D.; Duan, X. F. Rapid electrochemical cleaning silver nanowire thin films for high-performance transparent conductors. *J. Am. Chem. Soc.* **2019**, *141*, 12251–12257.

[16] Liu, J. F.; Ge, Y. J.; Zhang, D. M.; Han, M.; Li, M. X.; Zhang, M.; Duan, X. D.; Yang, Z. L.; Hu, J. W. Plasma cleaning and self-limited welding of silver nanowire films for flexible transparent conductors. *ACS Appl. Nano Mater.* **2021**, *4*, 1664–1671.

[17] Cui, Z.; Poblete, F. R.; Zhu, Y. Tailoring the temperature coefficient of resistance of silver nanowire nanocomposites and their application as stretchable temperature sensors. *ACS Appl. Mater. Interfaces* **2019**, *11*, 17836–17842.

[18] Chung, W. H.; Jang, Y. R.; Hwang, Y. T.; Kim, S. H.; Kim, H. S. The surface plasmonic welding of silver nanowires via intense pulsed light irradiation combined with NIR for flexible transparent conductive film. *Nanoscale* **2020**, *12*, 17725–17737.

[19] Liu, Y.; Zhang, J. M.; Gao, H.; Wang, Y.; Liu, Q. X.; Huang, S. Y.; Guo, C. F.; Ren, Z. F. Capillary-force-induced cold welding in silver-nanowire-based flexible transparent electrodes. *Nano Lett.* **2017**, *17*, 1090–1096.

[20] Kang, H.; Song, S. J.; Sul, Y. E.; An, B. S.; Yin, Z. X.; Choi, Y.; Pu, L.; Yang, C. W.; Kim, Y. S.; Cho, S. M. et al. Epitaxial-growth-

induced junction welding of silver nanowire network electrodes. *ACS Nano* **2018**, *12*, 4894–4902.

[21] Luo, B. B.; Fang, Y. S.; Li, J.; Huang, Z.; Hu, B.; Zhou, J. Improved stability of metal nanowires via electron beam irradiation induced surface passivation. *ACS Appl. Mater. Interfaces* **2019**, *11*, 12195–12201.

[22] Manikandan, A.; Lee, L.; Wang, Y. C.; Chen, C. W.; Chen, Y. Z.; Medina, H.; Tseng, J. Y.; Wang, Z. M.; Chueh, Y. L. Graphene-coated copper nanowire networks as a highly stable transparent electrode in harsh environments toward efficient electrocatalytic hydrogen evolution reactions. *J. Mater. Chem. A* **2017**, *5*, 13320–13328.

[23] Ahn, Y.; Jeong, Y.; Lee, Y. Improved thermal oxidation stability of solution-processable silver nanowire transparent electrode by reduced graphene oxide. *ACS Appl. Mater. Interfaces* **2012**, *4*, 6410–6414.

[24] Zhu, Y. Z.; Kim, S.; Ma, X. Z.; Byrley, P.; Yu, N.; Liu, Q. S.; Sun, X. M.; Xu, D.; Peng, S. S.; Hartel, M. C. et al. Ultrathin-shell epitaxial Ag@Au core–shell nanowires for high-performance and chemically-stable electronic, optical, and mechanical devices. *Nano Res.* **2021**, *14*, 4294–4303.

[25] Eom, H.; Lee, J.; Pichitpajongkit, A.; Amjadi, M.; Jeong, J. H.; Lee, E.; Lee, J. Y.; Park, I. Ag@Ni core–shell nanowire network for robust transparent electrodes against oxidation and sulfurization. *Small* **2014**, *10*, 4171–4181.

[26] Zhao, Y.; Wang, X. J.; Yang, S. Z.; Kuttner, E.; Taylor, A. A.; Salemmilani, R.; Liu, X.; Moskovits, M.; Wu, B. H.; Dehestani, A. et al. Protecting the nanoscale properties of Ag nanowires with a solution-grown SnO_2 monolayer as corrosion inhibitor. *J. Am. Chem. Soc.* **2019**, *141*, 13977–13986.

[27] Sohn, H.; Kim, S.; Shin, W.; Lee, J. M.; Lee, H.; Yun, D. J.; Moon, K. S.; Han, I. T.; Kwak, C.; Hwang, S. J. Novel flexible transparent conductive films with enhanced chemical and electromechanical sustainability: TiO_2 nanosheet-Ag nanowire hybrid. *ACS Appl. Mater. Interfaces* **2018**, *10*, 2688–2700.

[28] Su, D. Y.; Hsu, C. C.; Lai, W. H.; Tsai, F. Y. Fabrication, mechanisms, and properties of high-performance flexible transparent conductive gas-barrier films based on Ag nanowires and atomic layer deposition. *ACS Appl. Mater. Interfaces* **2019**, *11*, 34212–34221.

[29] Madeira, A.; Plissonneau, M.; Servant, L.; Goldthorpe, I. A. Tréguer-Delapierre, M. Increasing silver nanowire network stability through small molecule passivation. *Nanomaterials (Basel)* **2019**, *9*, 899.

[30] Liu, G. S.; Xu, Y. W.; Kong, Y. F.; Wang, L.; Wang, J.; Xie, X.; Luo, Y. H.; Yang, B. R. Comprehensive stability improvement of silver nanowire networks via self-assembled mercapto inhibitors. *ACS Appl. Mater. Interfaces* **2018**, *10*, 37699–37708.

[31] Yang, K. C.; Sung, D. I.; Shin, Y. J.; Yeom, G. Y. Highly oxidation-resistant silver nanowires by C_xF_y polymers using plasma treatment. *Nanotechnology* **2019**, *30*, 285702.

[32] Ning, Z. J.; Voznyy, O.; Pan, J.; Hoogland, S.; Adinolfi, V.; Xu, J. X.; Li, M.; Kirmani, A. R.; Sun, J. P.; Minor, J. et al. Air-stable n-type colloidal quantum dot solids. *Nat. Mater.* **2014**, *13*, 822–828.

[33] Chu, X. K.; Wang, K.; Tao, J. Q.; Li, S. X.; Ji, S. L.; Ye, C. H. Tackling the stability issues of silver nanowire transparent conductive films through $FeCl_3$ dilute solution treatment. *Nanomaterials (Basel)* **2019**, *9*, 533.

[34] Genlik, S. P.; Tigan, D.; Kocak, Y.; Ercan, K. E.; Cicek, M. O.; Tunca, S.; Koylan, S.; Coskun, S.; Ozensoy, E.; Unalan, H. E. All-solution-processed, oxidation-resistant copper nanowire networks for optoelectronic applications with year-long stability. *ACS Appl. Mater. Interfaces* **2020**, *12*, 45136–45144.

[35] Al-Saidi, W. A.; Feng, H. J.; Fichthorn, K. A. Adsorption of polyvinylpyrrolidone on Ag surfaces: Insight into a structure-directing agent. *Nano Lett.* **2012**, *12*, 997–1001.

[36] Mao, H. B.; Feng, J. Y.; Ma, X.; Wu, C.; Zhao, X. J. One-dimensional silver nanowires synthesized by self-seeding polyol process. *J. Nanopart. Res.* **2012**, *14*, 887.

[37] Dai, W. L.; Cao, Y.; Deng, J. F.; Liao, Y. Y.; Hong, B. F. The role of iodide promoter in selective oxidation of methanol to formaldehyde. *Catal. Lett.* **1999**, *63*, 49–57.

[38] Hsieh, Y. C.; Betancourt, L. E.; Senanayake, S. D.; Hu, E. Y.; Zhang, Y.; Xu, W. Q.; Polyansky, D. E. Modification of CO_2 reduction activity of nanostructured silver electrocatalysts by surface halide anions. *ACS Appl. Energy Mater.* **2019**, *2*, 102–109.

[39] Han, M.; Ge, Y. J.; Liu, J. F.; Cao, Z. Z.; Li, M. X.; Duan, X. D.; Hu, J. W. Mixed polyvinyl pyrrolidone hydrogel-mediated synthesis of high-quality Ag nanowires for high-performance transparent conductors. *J. Mater. Chem. A* **2020**, *8*, 21062–21069.

[40] Wang, D. M.; Hua, H. M.; Liu, Y.; Tang, H. R.; Li, Y. X. Single Ag nanowire electrodes and single Pt@Ag nanowire electrodes: Fabrication, electrocatalysis, and surface-enhanced Raman scattering applications. *Anal. Chem.* **2019**, *91*, 4291–4295.

[41] Wojclechowski, M.; Go, W.; Osteryoung, J. Square-wave anodic stripping analysis in the presence of dissolved oxygen. *Anal. Chem.* **1985**, *57*, 155–158.

[42] Yokota, Y.; Wong, R. A.; Hong, M. S.; Hayazawa, N.; Kim, Y. Monatomic iodine dielectric layer for multimodal optical spectroscopy of dye molecules on metal surfaces. *J. Am. Chem. Soc.* **2021**, *143*, 15205–15214.

[43] Elechiguerra, J. L.; Larios-Lopez, L.; Liu, C.; Garcia-Gutierrez, D.; Camacho-Bragado, A.; Yacaman, M. J. Corrosion at the nanoscale: The case of silver nanowires and nanoparticles. *Chem. Mater.* **2005**, *17*, 6042–6052.

[44] Yue, Y.; Liu, N. S.; Liu, W. J.; Li, M.; Ma, Y. N.; Luo, C.; Wang, S. L.; Rao, J. Y.; Hu, X. K.; Su, J. et al. 3D hybrid porous Mxene-sponge network and its application in piezoresistive sensor. *Nano Energy* **2018**, *50*, 79–87.

[45] Zheng, Y. J.; Yin, R.; Zhao, Y.; Liu, H.; Zhang, D. B.; Shi, X. Z.; Zhang, B.; Liu, C. T.; Shen, C. Y. Conductive MXene/cotton fabric based pressure sensor with both high sensitivity and wide sensing range for human motion detection and e-skin. *Chem. Eng. J.* **2021**, *420*, 127720.